Traffic & Transportation

Capturing the Impacts of Multi-Source Information under the V2X Environment Based on the Car-Following Model

Qing WANG[1], Meiying JIAN[2], Pengrui ZHAO[3], Qianwei NIU[4], Chengbing LI[5]

Original Scientific Paper
Submitted: 4 Mar 2025
Accepted: 16 July 2025
Published: 28 Apr 2026

[1] wangqing_0602@163.com, Institute of Transportation, Inner Mongolia University, Hohhot, China
[2] Corresponding author, jianmy@imu.edu.cn, Institute of Transportation, Inner Mongolia University, Hohhot, China
[3] zhaopengrui1016@163.com, Institute of Transportation, Inner Mongolia University, Hohhot, China
[4] nqw1013122871@163.com, Institute of Transportation, Inner Mongolia University, Hohhot, China
[5] bingbingnihao2008@126.com, Institute of Transportation, Inner Mongolia University, Hohhot, China

Publisher:
Faculty of Transport and Traffic Sciences, University of Zagreb

ABSTRACT
This study aims to establish an improved model framework for integrating the car-following information under the V2X environment and compare the contributions of various information. Based on the vehicle interaction information identified in the V2X environment, the improved model is established by integrating multi-source information, which includes preceding and following car position, velocity difference, accelerations of multiple preceding vehicles, adjacent vehicle optimal velocity difference and driver memory effect information, named BL-MSIF model. Then numerical simulation is used to validate the BL-MSIF model. The results indicate that the BL-MSIF model has excellent characteristics in enhancing traffic flow stability. In addition, based on numerical simulations, a comparative analysis of the contributions of various types of information in the BL-MSIF model is conducted from perspectives of traffic flow stability, additional energy consumption and traffic safety. It is found that the acceleration information of preceding vehicles holds the highest importance, while the contribution of driver memory effect information to the model is relatively low. The results of this study serve as a crucial benchmark for the practice and theory related to traffic flow in the V2X environment.

KEYWORDS
car-following model; sensitivity analysis; numerical simulation; traffic safety; traffic flow stability.

1. INTRODUCTION

The existing transportation supply has failed to meet the rapidly growing demand for traffic, resulting in a series of negative externalities in transportation activities, such as gridlock, collisions and environmental degradation caused by vehicles. To address these traffic issues, intelligent transport technologies are continually evolving and being updated. These novel technologies include vehicle-to-everything (V2X) communication technology [1-3], autonomous driving technology [4-6], and so on. However, due to technological maturity and the incomplete formulation of relevant laws and regulations, it is difficult for autonomous driving to be widely deployed in the short term [7]. V2X communication technology has a greater possibility of short-term application and operational deployment. Consequently, there is an urgent need to study micro-traffic flow in the V2X environment.

In the V2X environment, the level of informatisation in the traffic system is notably improved, and the driver-vehicle units' ability to perceive information is markedly strengthened. Connections and interactive relationships among multiple vehicles could be established. Then, extensive micro-traffic data from various vehicles in the system will be gathered, including their operational states (position, speed, acceleration, etc.)

[8]. This will unavoidably impact the vehicle motion, particularly in car-following behaviours. However, too much information may result in difficulty in decision-making among drivers. Information that should be captured is required for the investigation.

Numerous car-following models with different information based on V2X technology have been established. Sun et al. [9] introduced an enhanced car-following model derived from the optimal velocity (OV) model, which considered the influence of two consecutive leading vehicles. Peng et al. [10] developed an extended car-following framework based on the full velocity difference (FVD) model, incorporating interactions with two preceding vehicles and the adjacent following vehicle within a driver's field of view. Peng et al. [11] brought up a car-following model that integrated the historical evolution information integral (HEII) effect under the V2X environment, building on the OV model. Dangi and Redhu [12] proposed an improved car following model based on the full velocity difference model by considering the driver's memory and the influence of the V2X environment on the traffic flow system. Some studies [13,14] have established improved car-following models by considering the impact of cyberattacks in the V2X environment on traffic dynamics. Other studies [15-17] have also taken into account the influence of driver behaviours, such as driver attention and overtaking behaviour, and established a car following model in the V2X environment. Tang et al. [18] investigated the impact of V2X information on driver behaviour, showing that V2X technology enables drivers to respond more proactively to traffic conditions and reduces carbon dioxide emissions in the transportation system.

It can be seen that various information has been proposed and added to car-following models. However, previous studies focused on the effect of one or two information. With the help of V2X technology, considerable information from multiple vehicles can be obtained that may impact car-following behaviour. The new issues, such as whether all of these factors come into play in car-following behaviour, which factors are the most significant, and how to integrate these factors into car-following models, have not been addressed. On this basis, this paper focuses on the following three questions. Question 1 involves clarifying which traffic information, accessible to driver-vehicle units in the V2X environment, is considered valid for building car-following models. Question 2 is concerned with integrating the identified traffic information to establish car-following models based on the V2X environment. Then, the validation of the improved model is conducted through numerical experimentation. Question 3 involves evaluating the contribution of each information item in terms of traffic flow stability, safety and energy consumption. This research is dedicated to enhancing the stability and safety of traffic flow, and also provides a certain reference basis for the formulation of vehicle control strategies in the intelligent connected environment and the construction of simulation models in the traffic system.

2. RELATED WORK

This section reviews the improved car-following models within the V2X environment, clarifying the necessary valid information for establishing the models.

Lenz et al. [19] initiated the shift from bilateral to multilateral interactions in car-following models. Since then, researchers have built on this work by expanding traditional models to account for the motion state information of multiple preceding vehicles. Wang et al. [20] incorporated the speed differences among multiple preceding vehicles into their research and established the multiple velocity difference (MVD) model. Peng and Sun [21] considered multiple inputs of information from several preceding vehicles and proposed an improved multiple car-following (MCF) model. Sun et al. [22] introduced a car-following model that incorporates information on the positions and velocity differences of multiple preceding vehicles, named the multiple ahead & velocity difference (MAVD) model. Informed by the preceding models, simulations demonstrate that traffic data from multiple leading vehicles have a substantial effect on traffic flow characteristics.

Practical driving experience suggests that drivers monitor the motion states of vehicles behind them during the car-following process. Then Sun et al. [23] incorporated backwards-looking effects and integrated information from multiple preceding vehicles. Since then, numerous researchers have explored how the backwards-looking effect impacts traffic flow characteristics [24-27]. Approaching the topic from different perspectives, they have developed diverse traffic models and confirmed the crucial role of backwards-looking effects in stabilising traffic flow.

In addition, some researchers have also examined how the optimal velocity difference between adjacent and non-adjacent vehicles influences car-following behaviour. Peng et al. [28], by acquiring information on non-adjacent preceding vehicles, put forward the optimal velocity difference (OVD) model. Cao et al. [29]

expanded the OVD model by adding the optimal velocity adjustments from multiple preceding vehicles. This enhanced model considers the optimal velocity difference between adjacent vehicles, which significantly supports drivers in refining their car-following strategies.

Furthermore, several researchers have explored how acceleration factors influence traffic flow dynamics. Li et al. [30] developed the optimal velocity difference and acceleration (OVDA) model, integrating the acceleration data from the nearest preceding vehicle. Simulations revealed that this enhanced model can significantly extend the stability range of traffic flow. Yu and Shi [31] analysed real-world data and developed an enhanced car-following model that incorporates the acceleration of both leading vehicles. Their findings highlight the significance of acceleration information in constructing effective car-following models.

Moreover, Herman et al. [32] discovered that drivers maintain a recollection of past driving experiences during the driving process. Several researchers have explored how speed and headway dynamics change with driver memory incorporated into traffic flow models. Their findings indicate that accounting for driver memory notably improves traffic behaviour and stability [33-36]. With the V2X technology, the system can record vehicle evolution information over time. Then it is necessary to consider driver memory effects when establishing car-following models in the V2X environment.

In conclusion, all existing models introduce one or two information, involving motion states of multiple preceding vehicles, backwards-looking effects, optimal velocity difference, driver memory effects and acceleration factors. But with the development of V2X technology, more and more information will be perceived, and it will impact car-following behaviour collectively. Therefore, the integration of multi-source information is vital for enhancing car-following models in the V2X environment.

3. MODEL CONSTRUCTION WITH MULTI-SOURCE INFORMATION

This section presents an enhanced car-following model that incorporates multi-source information.

Generally, car following models refer to the relationship between stimulus and response. Here, the stimulus indicates information that a driver can obtain. In the V2X environment, this information includes motion states of multiple preceding vehicles, backwards-looking effects, optimal velocity difference, driver memory effects and acceleration factors, and these will be perceived. The response is always represented by the acceleration or deceleration of the following vehicle. Then the equation of car-following can be expressed as *Equation 1*;

$$\frac{dv_n(t)}{dt} = f\left(\sum_{j=1}^{K} \Delta x_{n+j-1}(t), \sum_{j=1}^{K} \Delta x_{n+j-1}(t-\tau), \Delta x_{n-1}(t), \Delta x_{n+1}(t), \sum_{j=1}^{K} \Delta v_{n+j-1}(t), \sum_{j=1}^{K} a_{n+j}(t)\right) \tag{1}$$

where $\Delta x_{n+1}(t)$ denotes the space headway between vehicles $(n+1)$ and $(n+2)$ at time t, $\Delta x_{n-1}(t)$ indicates the space headway between vehicles $(n-1)$ and n at time t, $\Delta x_{n+j-1}(t)$ and $\Delta x_{n+j-1}(t-\tau)$ are the spaces headway between vehicles $(n+j-1)$ and $(n+j)$ at time t and $(t-\tau)$, respectively. $\Delta v_{n+j-1}(t)$ is the velocity difference between vehicles $(n+j-1)$ and $(n+j)$ at time t. $a_{n+j}(t)$ represents the acceleration (declaration) of vehicle $(n+j)$.

Concerning the expression of stimulus-response function $f(\cdot)$, there have emerged nearly hundreds of models, such as the collision avoidance model [37], artificial neural network model [38], OV model, etc. Among them, as an improved OV model, the FVD model stands out as one of the most frequently utilised and well-studied models [39]. In the FVD model, it is suggested that the stimulus refers to the joint action of the optimal velocity item and velocity difference. The equation describing motion is presented as *Equation 2;*

$$\frac{dv_n(t)}{dt} = \alpha[V(\Delta x_n(t)) - v_n(t)] + \lambda \Delta v_n(t) \tag{2}$$

where α is the sensitivity factor. $V(\Delta x_n(t))$ represents the optimal velocity function and $\Delta x_n(t)$ means the space headway between vehicles n and $(n+1)$ at time t. $v_n(t)$ is the velocity of the n th vehicle at time t. $\Delta v_n(t)$ is the velocity difference between the leading and following vehicles, namely, $\Delta v_n(t) = v_{n+1}(t) - v_n(t)$, and λ is its sensitivity coefficient.

Similar to the forward-looking effect, the information of the following vehicle is also considered [23]. Then, the backwards-looking and velocity difference (BLVD) model [40] is proposed, as follows.

$$\frac{dv_n(t)}{dt} = \alpha[(1-p)V_F(\Delta x_n(t)) + pV_B(\Delta x_{n-1}(t)) - v_n(t)] + \lambda \Delta v_n(t) \tag{3}$$

where $V_F(\Delta x_n(t))$ is the optimal velocity with forward looking effect of the n th vehicle at time t, $V_B(\Delta x_{n-1}(t))$ is the optimal velocity with the backwards-looking effect of the $(n-1)$ th vehicle at time t, and p represents the attention weight to the backwards-looking effect.

Based on this BLVD model, the remaining information is incorporated to construct the improved model with V2X technology, named backwards-looking and multi-source information fusion (BL-MSIF) model. Given the advantages of linear models, such as concise representation, strong interpretability and robust generalisation capabilities, all the factors are integrated in the form of a linear weighted sum. Then the improved BL-MSIF model can be expressed as follows;

$$\begin{aligned}\frac{dv_n(t)}{dt} = {} & \alpha[(1-p)V_F(\Delta x_n(t)) + pV_B(\Delta x_{n-1}(t)) - v_n(t)] + \lambda \sum_{j=1}^{K} q_j \, \Delta v_{n+j-1}(t) + \beta[V_F(\Delta x_{n+1}(t)) - V_F(\Delta x_n(t))] \\ & + \omega \sum_{j=1}^{K} \eta_j a_{n+j}(t) + \gamma \sum_{j=1}^{K} \xi_j \left[V_F\left(\Delta x_{n+j-1}(t)\right) - V_F\left(\Delta x_{n+j-1}(t-\tau)\right)\right], j = 1,2,\cdots,K; K \ll N\end{aligned} \tag{4}$$

where the first item refers to the backwards-looking effect, the second item refers to the velocity difference information of multiple preceding vehicles. The third item considers the optimal velocity difference information of adjacent vehicles. The fourth item is the acceleration information of multiple preceding vehicles. The fifth item indicates the driver's memory effect on the current vehicle's operating state. While it has been established that incorporating memory into both velocity and headway variables enhances traffic flow stability, drivers may also adapt their anticipation of optimal velocity based on the memory-influenced changes in optimal velocity [35]. Then this study considers the optimal velocity that changes with memory.

The variables and symbols for the equations are described in *Table 1*.

Table 1 – Description of variables and symbols

Variables/Symbols	Description
$V_F(\Delta x_{n+1}(t))$	The optimal velocity with forward-looking effect of the $(n+1)$ th vehicle at time t.
$V_F\left(\Delta x_{n+j-1}(t)\right)$	The optimal velocity with forward-looking effect of the $(n+j-1)$ th vehicle at time t.
$V_F\left(\Delta x_{n+j-1}(t-\tau)\right)$	The optimal velocity with forward-looking effect of the $(n+j-1)$ th vehicle at time $t-\tau$.
β	The sensitivity coefficient of the optimal velocity difference term.
ω	The sensitivity coefficient of the acceleration term.
γ	The sensitivity coefficient of the driver memory effect term.
τ	Sampling time interval.
K	The number of leading vehicles perceivable in the V2X environment, $K \in N$.
q_j	The weight coefficient of the velocity difference term for the $4th$ vehicle.
η_j	The weight coefficient of the acceleration term for the $4th$ vehicle.
ξ_j	The weight coefficient of the driver memory effect term for the $4th$ vehicle.
q_j, η_j, ξ_j	$q_j = \eta_j = \xi_j = \begin{cases} \frac{K-1}{K^j}, j \neq K \\ \frac{1}{K^{j-1}}, j = K \end{cases}$, $\sum_{j=1}^{K} q_j = \sum_{j=1}^{K} \eta_j = \sum_{j=1}^{K} \xi_j = 1$.

For the improved car-following BL-MSIF model established above, the utilised optimal velocity function is represented by *Equation 5.*

$$V_F(\Delta x_n(t)) = \alpha'[tanh(\Delta x_n(t) - h_c) + tanh(h_c)]$$
$$V_B(\Delta x_{n-1}(t)) = -\alpha''[tanh(\Delta x_{n-1}(t) - h_c) + tanh(h_c)] \quad (5)$$

where α', α'' are positive constants, h_c is the safe distance.

To simplify computations, neglecting the nonlinear terms in the Taylor expansion of the variable $\Delta x_n(t-\tau)$, the simplified calculation for $\Delta x_n(t-\tau)$ is given by *Equation 6*:

$$\Delta x_n(t-\tau) = \Delta x_n(t) - \tau\frac{dv_n(t)}{dt} = \Delta x_n(t) - \tau\Delta v_n(t) \quad (6)$$

Similarly, the simplified expression for $V_F(\Delta x_n(t-\tau))$ is shown in *Equation 7*:

$$V_F(\Delta x_n(t-\tau)) = V_F(\Delta x_n(t)) - \tau\Delta v_n(t)V_F'(\Delta x_n(t)) \quad (7)$$

Substituting *Equations 6* and *7* into *Equation 4* yields the simplified motion equation, as shown in *Equation 8*:

$$\frac{dv_n(t)}{dt} = \alpha[(1-p)V_F(\Delta x_n(t)) + pV_B(\Delta x_{n-1}(t)) - v_n(t)] + \lambda\sum_{j=1}^{K} q_j\,\Delta v_{n+j-1}(t) + \beta[V_F(\Delta x_{n+1}(t)) - V_F(\Delta x_n(t))]$$
$$+ \gamma\tau\sum_{j=1}^{K}\xi_j V_F'\left(\Delta x_{n+j-1}(t)\right)\Delta v_{n+j-1}(t) + \omega\sum_{j=1}^{K}\eta_j a_{n+j}(t), j = 1,2,\cdots,K; K \ll N \quad (8)$$

4. ESTIMATION OF MODEL KEY PARAMETERS

As shown in *Equation 8*, many parameters need to be estimated. Fortunately, some of them, such as α, λ, ω, τ and γ, have been discussed in previous studies [22, 23]. Then these parameters in the model are taken as a reference to the empirical value, as shown in *Table 2*. The other three critical parameters, the sensitivity coefficient of optimal velocity difference β, the number of leading vehicles K and the weight parameter of backwards-looking effect p, need to be estimated. To this end, the impact of these three parameters on the stability of connected vehicle traffic flow is analysed by numerical simulations. Vehicle speed and headway are used as performance indicators. Based on these, the optimal values of parameters β, K and p are determined.

Table 2 – The critical parameters for model simulation

Parameter names and symbols	Values
Sampling time interval τ	0.2s
The sensitivity coefficient α	0.41
The sensitivity coefficient λ	0.5
The sensitivity coefficient ω	0.3
The sensitivity coefficient γ	0.2

In the simulation experiment, a circular road is designed with a total length of $L = 400\ m$. A hundred vehicles are uniformly distributed with identical inter-vehicle spacing. The experimental vehicles are numbered from 1 to 100, with the second vehicle following the first, and so on, forming a circular arrangement where the front car of the 100th vehicle is the 1st vehicle. The initial conditions for vehicles are as follows:

$$\begin{cases} x_1(0) = 1m \\ x_n(0) = (n-1)L/N, (n = 2,3,\cdots,N) \\ v_n(0) = (1-p)V_F(L/N) + pV_B(L/N), (n = 1,2,\cdots,N) \end{cases} \quad (9)$$

A vehicle disturbance simulation experiment was conducted by introducing a disturbance variable to observe the operating status of the entire vehicle platoon, as shown in *Algorithm 1*.

Algorithm 1 – The main steps of the simulation disturbance experiment

Input: Initial states of vehicles (position $x_n(0)$, velocities $v_n(0)$ etc.), disturbance variable ΔL, time step $\Delta t = 0.2s$, total number of vehicles $N = 100$.

Output: State information (positions, velocities, etc. over time) of all vehicles after being affected by the disturbance.

Step 1. Introduce a disturbance variable ΔL
function introduce disturbance ()
$x_1(1) = x_1(t) + \Delta L$ // Introduce the disturbance term to vehicle 1
return x_1
end
Step 2. Calculate the headway distance after introducing the disturbance
function calculate headway distance ()
for n from 1 to $N - 1$
$\Delta x_n(1) = x_{n+1}(1) - x_n(1)$
end for
return Δx_n
end
Step 3. Calculate the optimal velocity
function calculate optimal velocity (Δx_n)
for n from 1 to N
$V(\Delta x_n)$ = Calculate according to the optimal velocity equation (Δx_n) // Substitute Δx_n into the optimal velocity equation to calculate
end for
return $V(\Delta x_n)$
end
Step 4. Calculate the acceleration (or deceleration)
function calculate acceleration $V(\Delta x_n)$
for n from 1 to N
$a(n)$= Calculate the acceleration based on $V(\Delta x_n)$ // Calculate the acceleration using the optimal velocities obtained in Step 3
end for
return $a(n)$
end
Step 5. Update vehicle information
function update vehicle information **(**$a(n), v(n), x(n)$)
for n from 1 to N
$v(n) = v(n) + a(n)\Delta t$
$x(n) = x(n) + v(n)\Delta t + \frac{1}{2}a_n(t)\Delta t^2$
end for
return $v(n), x(n)$
end
Main simulation process
x_1 = introduce disturbance ()
while the number of disturbed vehicles $< N$ // Stop when all 100 vehicles are affected by the disturbance
Δx_n = calculate headway distance ()
$V(\Delta x_n)$ = calculate optimal velocity (Δx_n)
$a(n)$= calculate acceleration ($V(\Delta x_n)$)
$v(n), x(n)$ = update vehicle information ($a(n), v(n), x(n)$)
end while
return final state information of all vehicles ($v(n), x(n)$, etc.)

1) Estimation of parameter β

Impact of the sensitivity coefficient β for optimal velocity difference between adjacent vehicles on the velocity fluctuation characteristics of the vehicles. The number of leading vehicles K remained at its initial empirical value of 2, and the backwards-looking effect sensitivity coefficient p remained at its initial empirical value of 0.2, the sensitivity coefficient β ranges from [0,0.1,0.2,0.3] and other parameters were set according to *Table 2*. The results are shown in *Table 3*. In the *Table 3*, $R_{up} = \frac{v_{max} - v_{ave}}{v_{ave}}$ and $R_{dn} = \frac{v_{ave} - v_{min}}{v_{ave}}$ represents the

upward and the downward fluctuation of the velocity, respectively. $R_{ave} = \frac{v_{ave}-v_{min}}{v_{ave}}$ is the average of upward and downward fluctuation, which can comprehensively reflect the overall level of velocity fluctuations.

Table 3 – Velocity fluctuation characteristics under different β influences

β value	$v_{max}/(m \cdot s^{-1})$	$v_{ave}/(m \cdot s^{-1})$	$v_{min}/(m \cdot s^{-1})$	$R_{up}/\%$	$R_{dn}/\%$	$R_{ave}/\%$
0	0.69	0.60	0.49	14.99%	18.84%	16.92%
0.1	0.67	0.60	0.51	11.37%	14.95%	13.16%
0.2	0.67	0.60	0.53	11.29%	10.94%	11.12%
0.3	0.86	0.60	0.36	44.00%	40.60%	42.30%

From *Table 3*, it is evident that when β is set to 0.2, the average velocity fluctuation rate is smaller compared to other values of β. When β is equal to 0.2, the upward fluctuation rate R_{up} and downward fluctuation rate R_{dn} of velocity are 11.29% and 10.94%, respectively, resulting in an average fluctuation rate R_{ave} of 11.12%. This is lower than the scenarios when β is set to 0, 0.1 and 0.3. Therefore, introducing the optimal velocity difference between adjacent vehicles enhances the stability of traffic flow, and a value of β equal to 0.2 provides a better description for the model.

2) Estimation of parameter K

Impact of the multiple preceding vehicles K on the velocity fluctuation characteristics of the vehicles. Based on the simulation results from parameter sensitivity analysis 1, where β was set to 0.2, a sampling interval of 500 was utilised. The backwards-looking effect sensitivity coefficient p remained at its initial empirical value of 0.2, and other parameters were set according to *Table 2*. The simulation considered the acquisition of relevant driving information from 1 to 10 preceding vehicles (K=1,2,3,4,5,10) for the following car. According to the simulation experiment logic in *Algorithm 1*, a disturbance was applied to Vehicle 1, and the velocity fluctuations of Vehicles 90, 80, 70 and 60 were selected as the subjects of study. The simulation results are presented in *Figure 1*.

From *Figure 1*, it is evident that the speed fluctuation is the largest when $K = 1$, with peak-to-valley differences of 0.011, 0.005, 0.003 and 0.002 $m \cdot s^{-1}$ for the four vehicles, respectively. When $K = 2$, the vehicle speed fluctuation is the smallest, and the peak-valley differences of the four vehicles are 0.007, 0.003, 0.002 and 0.001 $m \cdot s^{-1}$ respectively. The speed of vehicles in the networked vehicle formation fluctuates, but the number of vehicles in front of K is not the bigger, the better. Therefore, setting $K = 2$ in the model contributes to enhancing the stability of traffic flow.

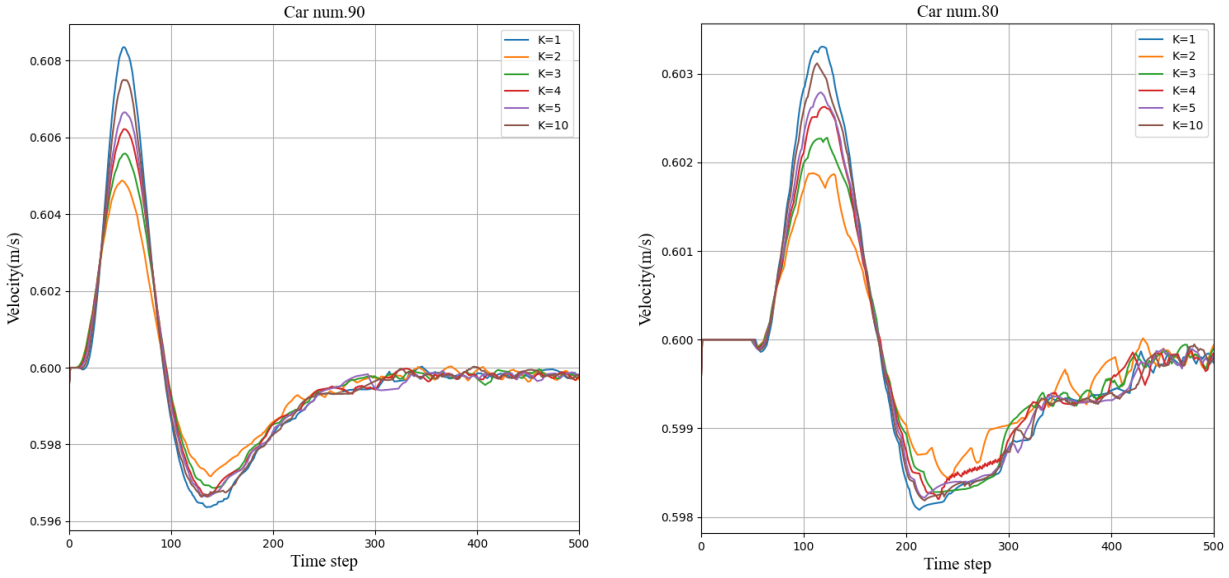

(a) *(b)*

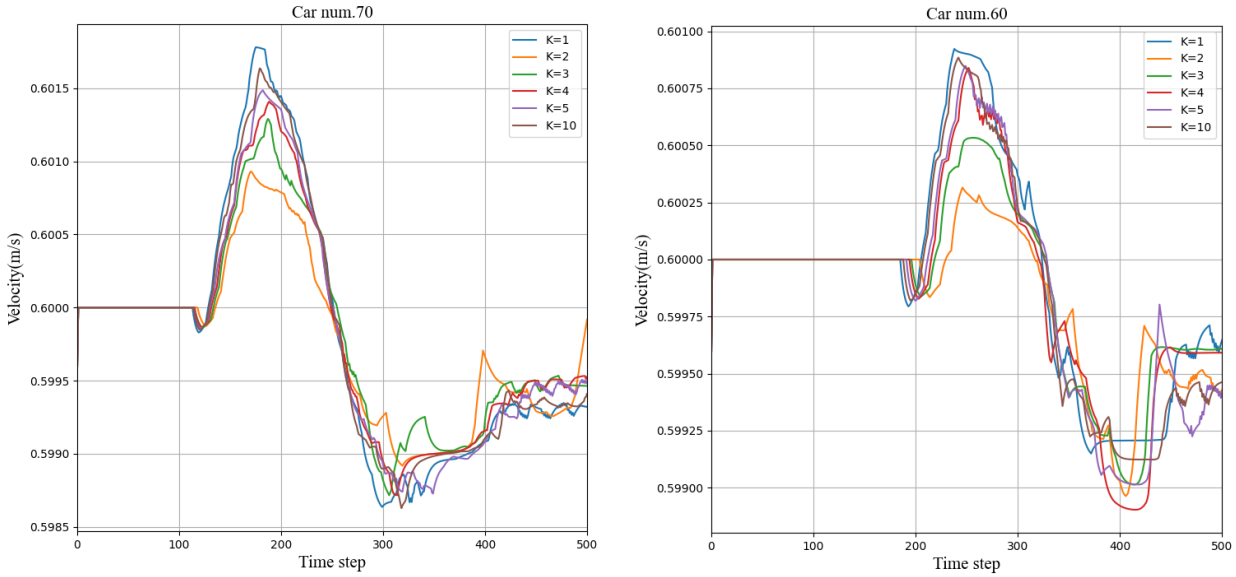

(c) *(d)*

Figure 1 – Velocity distribution of vehicles for different K values: a) Velocity distribution of car 90; b) Velocity distribution of car 80; c) Velocity distribution of car 70; d) Velocity distribution of car 60

3) Estimation of parameter p

Impact of the backwards-looking effect sensitivity coefficient p on the headway fluctuation characteristics. Based on the simulation results from parameter sensitivity analysis 1 and 2, with $\beta = 0.2$ and $K = 2$, and considering parameter p according to *Table 2*, numerical simulations were conducted to obtain headway distributions under different values of p, which range from [0,0.1,0.2,0.3], as illustrated in *Figure 2*. When $p = 0$, the headway density is maximised, and as p increases, the fluctuation of headway first decreases and then intensifies. Specifically, when $p = 0.2$, the headway fluctuation is most stable. Within 1,000 sampling intervals, the headway fluctuation variances for p values of 0, 0.1, 0.2 and 0.3 are 74.05, 17.26, 2.71 and 11.81 m, respectively. Therefore, introducing optimal velocity information from backwards-looking can enhance the stability of traffic flow, with further reduction in headway fluctuation when $p = 0.2$.

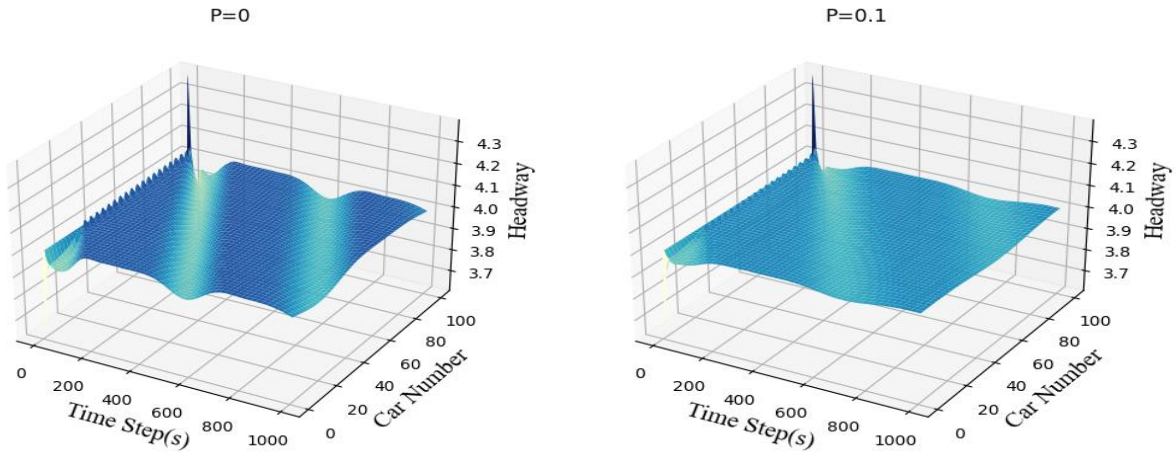

(a) *(b)*

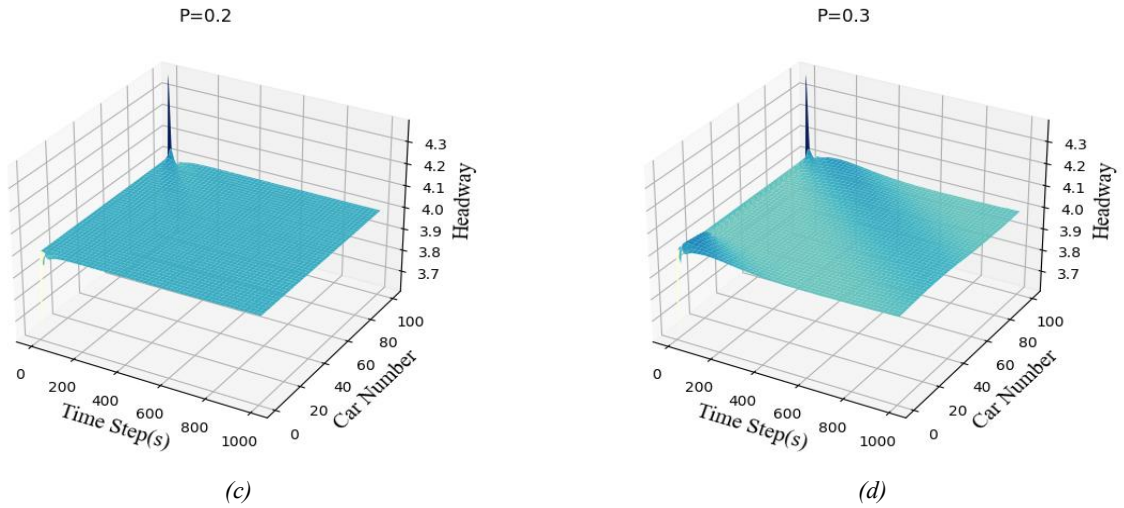

(c) *(d)*

Figure 2 – Headway distributions corresponding to different p *values: a)* $p = 0$*; b)* $p = 0.1$*; c)* $p = 0.2$*; d)* $p = 0.3$

5. VALIDATION OF BL-MSIF MODEL

The performance of the BL-MSIF model, which integrates multi-source information, is assessed by utilising numerical simulation.

To further validate the model for generalisability, four existing models are listed here for comparison with the BL-MSIF model, including the FVD model, BLVD, BL-OVD and BL-OVCM. Here, the BL-OVD model is a backwards-looking & optimal velocity difference model built upon the OVD model, and the BL-OVCM model is proposed based on the BLVD model, incorporating both backwards-looking effect and optimal velocity memory effects [41]. This section constructs two simulation scenarios, namely the circular road and the straight road, to verify the BL-MSIF model. The combination of circular and straight road scenarios has constructed a multi-dimensional verification framework from the two dimensions of closed-loop interaction and linear following. The circular scene emphasises the cumulative effect of disturbances in a periodic environment and is suitable for evaluating the long-term stability and collaborative control ability of the model. The straight scenario highlights the model's response efficiency to instantaneous sudden changes by simplifying the road conditions. By comparing the simulation results in the two types of scenarios, the performance of the BL-MSIF model under different traffic pressures can be comprehensively quantified, providing theoretical support for its application.

5.1 Simulation of the circular road scenario

In the simulation of the circular roads scenario, the established circular road scenario and simulation results from Section 4 ($\beta = 0.2, K = 2, p = 0.2$) are used. Furthermore, two different experimental scenes were designed: high-density and low-density. These scenes aim to investigate the BL-MSIF model's performance under varying conditions. The scene designs are outlined in *Table 4*.

According to *Algorithm 1*, a disturbance was applied to Vehicle 1, and then the operating status of the entire vehicle platoon was observed.

The output of the simulation results for scenes 1 and 2 is shown in *Figure 3*. As seen in *Figure 3a*, in high-density scenarios, the stability of BL-MSIF is the best. But from *Figure 3b*, it can be observed that all four models are relatively stable as the simulation time increases, and further analysis requires a detailed examination of the simulation data. Therefore, the velocity fluctuation characteristics at 500 sampling intervals are depicted in *Table 4*.

Table 4 – Design of different scenes

Control factors	Scenes	
	Scene 1	Scene 2
Road length/ m	400	10000
Number of vehicles/ veh	100	100
Traffic density	High density	Low density
Safe distance h_c	4m	30m

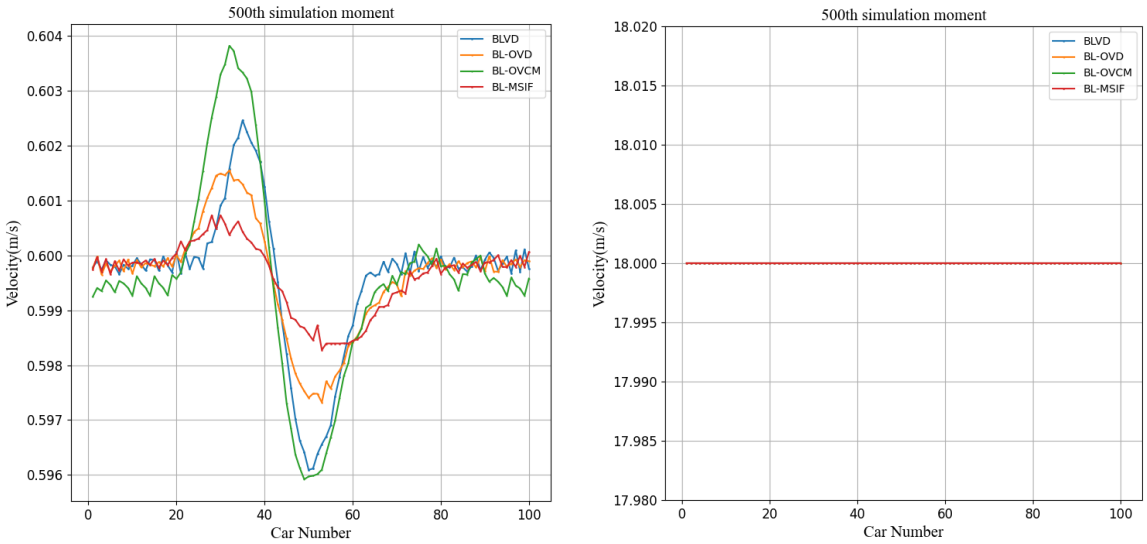

(a) *(b)*

Figure 3 – Velocity distribution of various models in different scenes: a) Scene 1 velocity distribution; b) Scene 2 velocity distribution

It can be observed that the BL-MSIF model exhibits a velocity fluctuation peak-to-valley difference of 0.002 $m \cdot s^{-1}$, consistently lower than the peak-to-valley values of the other three models (0.006 $m \cdot s^{-1}$, 0.004 $m \cdot s^{-1}$, 0.007 $m \cdot s^{-1}$). Additionally, the average velocity fluctuation rate of the BL-MSIF model is 0.02%, also consistently lower than the rates of the other models (0.05%, 0.04%, 0.07%). Similarly, in scene 2, the velocity fluctuation characteristics at 500 sampling intervals are shown in *Table 5*; the BL-MSIF model shows the best stability.

Table 5 – Simulation results of velocity fluctuation characteristics

Models	Scene 1				Scene 2			
	$v_{ave}/(m \cdot s^{-1})$	$v_{pt}/(m \cdot s^{-1})$	$R_{ave}/\%$	$D_v/(m \cdot s^{-1})$	$v_{ave}/(m \cdot s^{-1})$	$v_{pt}/(m \cdot s^{-1})$	$R_{ave}/\%$	$D_v/(m \cdot s^{-1})$
BLVD	0.600	0.006	0.05%	0.0002	18.00	$1.78\,e^{-14}$	$4.93\,e^{-16}$	$8.04\,e^{-15}$
BL-OVD	0.600	0.004	0.04%	0.0002	18.00	$1.78\,e^{-14}$	$4.93\,e^{-16}$	$8.04\,e^{-15}$
BL-OVCM	0.600	0.007	0.07%	0.0002	18.00	$1.42\,e^{-14}$	$3.95\,e^{-16}$	$6.12\,e^{-15}$
BL-MSIF	0.600	0.002	0.02%	$9.8\,e^{-5}$	18.00	$1.07\,e^{-14}$	$2.96\,e^{-16}$	$4.91\,e^{-15}$

The findings from the experiments show that the improved BL-MSIF model established in this study demonstrates excellent performance in maintaining stable traffic flow under varying traffic densities. The data suggest that this model offers better stability in acceleration and exerts more precise control over velocity changes when counteracting and absorbing disturbances.

5.2 Simulation of the straight road scenario

In the straight road simulation, the starting and braking simulation processes were designed to comprehensively verify the performance of the BL-MSIF following model.

1) Simulation of vehicle starting

The starting process of a vehicle simulates the process in which the traffic light changes from red to green in actual traffic conditions. The starting simulation scenario is a queue of 5 vehicles with a road length of L, where the first vehicle is numbered 1 and the remaining 4 vehicles are arranged in sequence at a headway of $\Delta x = 7.4\,m$. At the initial moment $t = 0$, the velocity of all vehicles is 0 $\mathrm{m \cdot s^{-1}}$. The lead vehicle starts at $t = 0$ with an acceleration of 3 $\mathrm{m \cdot s^{-2}}$. During the acceleration phase, the acceleration gradually decays. When the acceleration drops to 0, the lead vehicle maintains a constant speed of 12 $\mathrm{m \cdot s^{-1}}$. The first 5 vehicles in the queue are initially at rest when $t = 0$. When the leading vehicle starts to accelerate, the subsequent vehicles adopt the following behaviour according to the logic of the model. The initial position, velocity and acceleration of the vehicle during the starting process are set as follows.

$$\begin{cases} x_n(0) = (n-1)\Delta x_n, n = 1,2\cdots 5 \\ v_n(0) = 0, n = 1,2\cdots 5 \\ a_n(0) = \begin{cases} 3, n = 1 \\ 0, n = 2\cdots 5 \end{cases} \end{cases} \tag{10}$$

After the lead vehicle starts, all the vehicles follow the dynamic equation of the following model. During the movement of the vehicles, the driving state of the entire convoy is observed and recorded. Based on the above simulation scenario design, the BLVD model, BL-OVD model, BL-OVCM model and BL-MSIF model were simulated in the vehicle starting simulation scenario. The vehicle velocity distribution curves of the four models during the starting process are shown in *Figure 4*.

During the vehicle starting simulation process, the vehicle starting velocity of four different models and the time required for the entire vehicle fleet to reach a stable state were statistically analysed. The starting wave speed is calculated using $c_j = \Delta x_n / \delta t$, where δt represents the driving delay of the vehicle. The vehicle starting velocity of the BLVD model, BL-OVD model, BL-OVCM model and BL-MSIF model are calculated to be 5.12 $\mathrm{m \cdot s^{-1}}$, 5.31 $\mathrm{m \cdot s^{-1}}$, 5.99 $\mathrm{m \cdot s^{-1}}$ and 6.52 $\mathrm{m \cdot s^{-1}}$ respectively. From this, it can be seen that the BL-MSIF model has the largest starting velocity. As can be seen from *Figure 4d*, the time required for the entire vehicle fleet in the BL-MSIF model to reach a stable state is 15.3 s. For the three models in *Figures 4a-4c*, the time required for the entire vehicle fleet to reach a stable state is 24.6 s, 18.1 s and 16.5 s, respectively. This indicates that compared with the other three models, the BL-MSIF model can improve the vehicle starting efficiency and can efficiently transmit vehicle information, thus enhancing the response efficiency of the entire vehicle fleet.

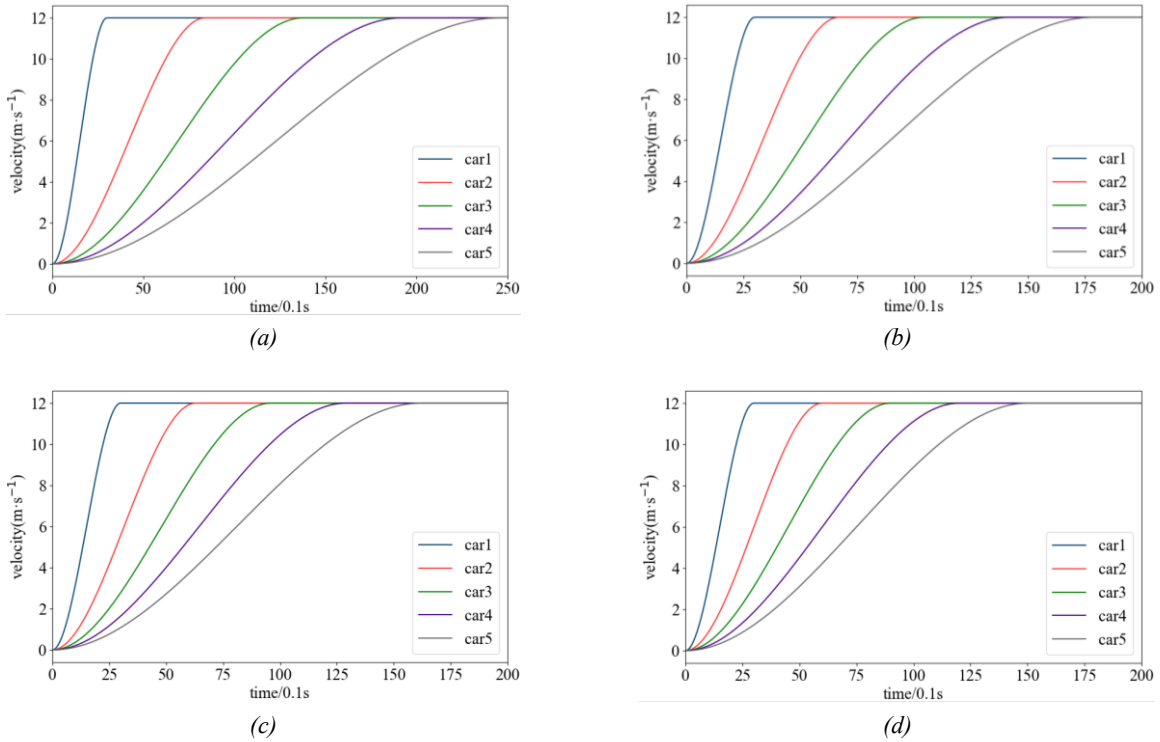

Figure 4 – Velocity distribution of various models during the vehicle's starting process: a) Velocity distribution of the BLVD model; b) Velocity distribution of the BL-OVD model; c) Velocity distribution of the BL-OVCM model; d) Velocity distribution of the BL-MSIF model

2) Simulation of vehicle braking

The braking process of a vehicle simulates the process in which the traffic light changes from green to red in actual traffic conditions. The simulation scene design of the braking process is as follows. In the initial state, five vehicles travel at a constant initial velocity of 12 $\mathrm{m} \cdot \mathrm{s}^{-1}$. At $t = 0$, the leading vehicle decelerates with an acceleration of -3 $\mathrm{m} \cdot \mathrm{s}^{-2}$. When the value of the acceleration decreases to 0, the velocity of the leading vehicle also becomes 0. When the lead vehicle slows down, the other four following vehicles in the convoy slow down in sequence. Other relevant parameters are consistent with the simulation scene design of the vehicle's starting process. The vehicle velocity distribution curves of the four models during the braking process are shown in *Figure 5*.

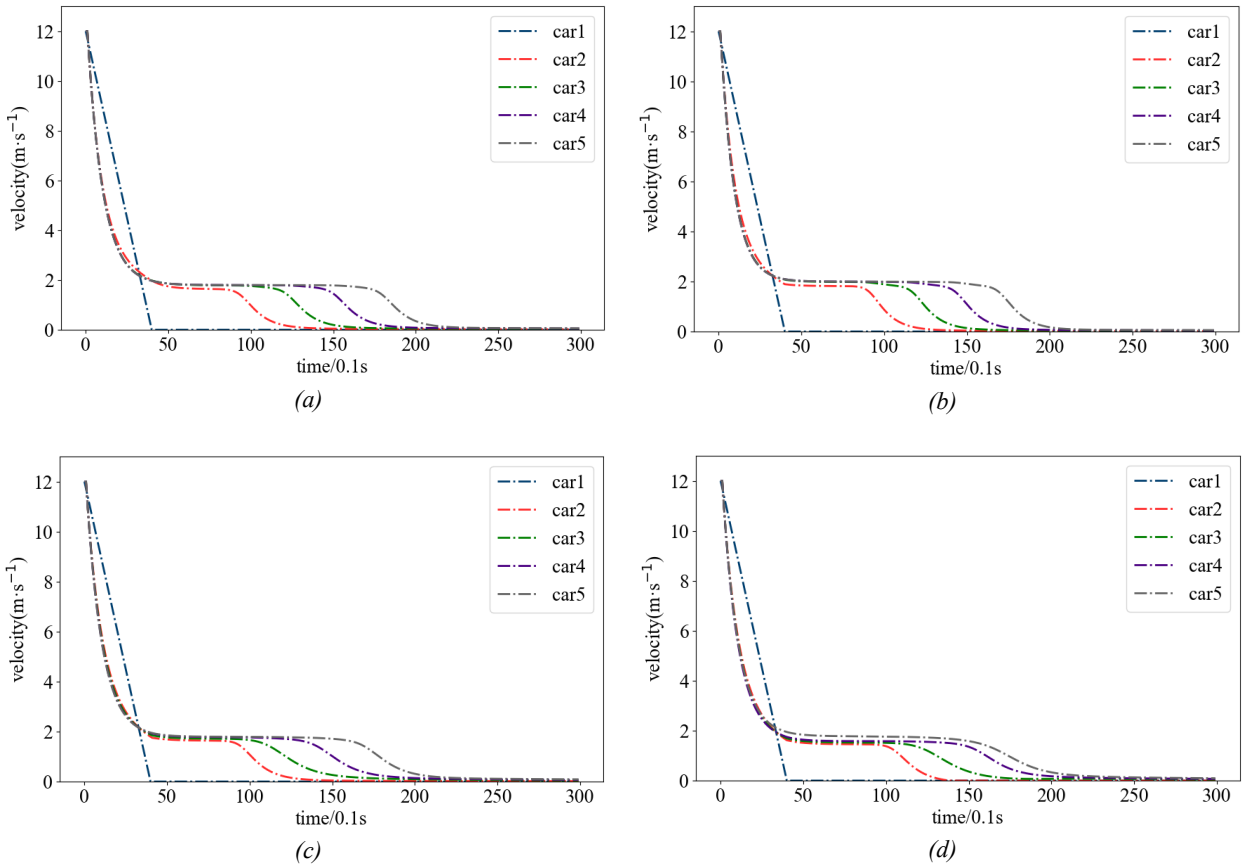

Figure 5 – Velocity distribution of various models during the vehicle's braking process: a) Velocity distribution of the BLVD model; b) Velocity distribution of the BL-OVD model; c) Velocity distribution of the BL-OVCM model; d) Velocity distribution of the BL-MSIF model

Through simulation, the time it takes for the entire fleet velocity to decrease to 0 during braking for four different models can be obtained. The time it takes for the vehicles of the four models from deceleration to stop in *Figures 5a-5d* is 26.8 s ,25.2 s, 23.6 s and 22.1 s, respectively. It can be seen from *Figure 5d* that during the braking process, the velocity fluctuation of the vehicle in the BL-MSIF model is relatively small, and the braking process can be achieved more smoothly.

6. ANALYSIS OF INFORMATION ITEMS OF THE MODEL

Based on the BL-MSIF model, the contributions of the information items are further analysed. To address this issue, the evaluation indicators need to be determined. As intelligent technology advances, many studies have focused on the stability of mixed traffic with cooperative adaptive cruise control (CACC), adaptive cruise control (ACC) and human vehicle [42, 43]. In addition, traffic safety as well as energy consumption and emissions are also common indicators for evaluating the impact of traffic modifications [44-47]. Then the importance of each information item is assessed from three perspectives: traffic flow stability, additional energy consumption and traffic safety.

Given that the BL-MSIF model is an improvement upon the BLVD model, the contribution of the adjacent vehicle optimal velocity difference, acceleration of multiple leading vehicles and driver memory information was analysed. Therefore, the BL-MSIF model in Section 3 is rewritten as follows.

$$\frac{dv_n(t)}{dt} = \alpha[(1-p)V_F(\Delta x_n(t)) + pV_B(\Delta x_{n-1}(t)) - v_n(t)] + \lambda\sum_{j=1}^{K} q_j\,\Delta v_{n+j-1}(t) + \kappa_1\beta[V_F(\Delta x_{n+1}(t)) - V_F(\Delta x_n(t))] + \kappa_2\omega\sum_{j=1}^{K}\eta_j a_{n+j}(t) + \kappa_3\gamma\tau\sum_{j=1}^{K}\xi_j V_F{}'\big(\Delta x_{n+j-1}(t)\big)\,\Delta v_{n+j-1}(t), j = 1,2,\cdots,K; K \ll N \quad (11)$$

here, $\kappa_x(x = 1,2,3)$ are all binary variables ranging from 0 to 1.

Based on the above analysis and the information items, three models are designed for simulation experiments. The design of the detailed expression of each model is shown in *Table 6* as follows.

Table 6 – The design of models for the analysis of the contribution of information items

Model	κ_x values		
	κ_1	κ_2	κ_3
Model A	1	1	0
Model B	1	0	1
Model C	0	1	1

6.1 Contribution to traffic flow stability

Velocity fluctuation characteristics of three models (Model A, B and C) are shown in *Table 7*. The peak-to-valley velocity difference of Model A is 0.0025 $m \cdot s^{-1}$, consistently lower than the peak-to-valley values of Model B and Model C (0.0037 $m \cdot s^{-1}$, 0.0030 $m \cdot s^{-1}$). The average velocity fluctuation rate of Model A is 0.21%, also consistently lower than the rates of Model B and Model C (0.31%, 0.25%). From this conclusion, by comparing the average fluctuation rates of each model's velocity individually, the contributions of the adjacent vehicle optimal velocity difference (κ_1 item), multiple leading vehicles acceleration (κ_2 item), and driver memory information (κ_3 item) can be obtained. Due to the smaller average velocity variation in the model, the importance of the missing information item is lower. It can be observed that the acceleration information of multiple leading vehicles is the most important, whereas the driver memory information item contributes relatively less.

Table 7 – Simulation results for Models A, B and C

Models	$v_{ave}/(m \cdot s^{-1})$	$v_{pt}/(m \cdot s^{-1})$	$R_{ave}/\%$
Model A	0.600	0.0025	0.21%
Model B	0.600	0.0037	0.31%
Model C	0.600	0.0030	0.25%

6.2 Contribution to additional energy consumption

If a vehicle maintains a consistent speed, its kinetic energy can remain stable, resulting in minimal additional energy consumption. Conversely, if the vehicle's speed undergoes significant changes over time, requiring frequent acceleration during the travel process, the additional energy consumption will sharply increase [48]. Moreover, in real-world traffic scenarios, a substantial rise in vehicle energy consumption typically occurs during the acceleration phase [49]. Based on this, the calculation for the additional energy consumption per vehicle is expressed in *Equation 12*;

$$\Delta E_n = \sum_t \delta_t \frac{1}{2}[v_n^2(t+1) - v_n^2(t)] \quad (12)$$

where δ_t is a variable factor, when $v_n(t+1) > v_n(t)$, $\delta_t = 1$, otherwise $\delta_t = 0$.

Hence, the total additional energy consumption for the entire transport system can be calculated as follows:

$$\Delta E = \sum_{n=1}^{N} \Delta E_n \tag{13}$$

Based on this, the additional energy consumption for the vehicles in the three models within 3,000 simulated time steps was calculated separately for scene 1 and scene 2. The results of the calculations are presented in *Figure 6*.

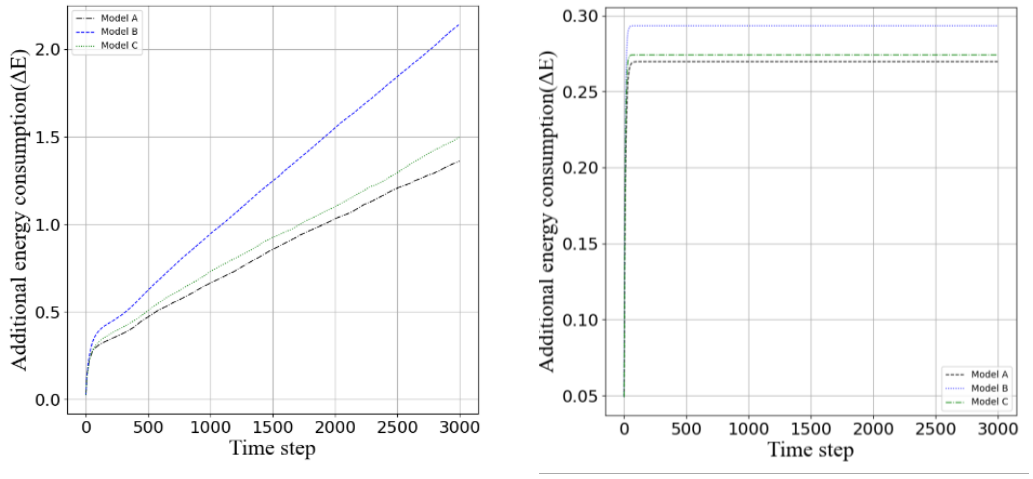

(a) *(b)*

Figure 6 – Additional energy consumption for various models in different scenes: a) The additional energy consumption within 3,000 simulated seconds for scene 1; b) The additional energy consumption within 3,000 simulated seconds for scene 2

From *Figure 6*, it is evident that in scene 1, i.e. under high density, Model A exhibits the minimum additional energy consumption over the 3,000 simulated moments collected, and Model B is the maximum. In scene 2, i.e. under low density, as the simulation moments increase, the additional energy consumption of Model A remains consistently lower than the other three models. Meanwhile, the additional energy consumption of Model B is always higher than that of the other two models. Since higher energy consumption indeed signifies the greater importance of the information items, the experimental findings once again demonstrate that the multiple leading vehicles' acceleration information item is the most important, whereas the driver memory information item contributes relatively less.

6.3 Contribution to traffic safety

To analyse the traffic flow safety in each model, this paper selects the time index TTC (time-to-collision). TTC measures the time before a collision might happen between a leading and a following vehicle, given that the speed difference is kept constant. The formula for TTC for vehicle n, at time t is provided in *Equation 14*.

$$TTC_n(t) = \begin{cases} \dfrac{\Delta x_n(t)}{v_n(t) - v_{n+1}(t)}, v_n(t) > v_{n+1}(t) \\ \infty, \ v_n(t) \leq v_{n+1}(t) \end{cases} \tag{14}$$

A lower TTC value signifies an increased likelihood of a rear-end collision at time t. However, TTC has limitations and time instability. Therefore, two indicators were introduced, namely time exposed to TTC below threshold (TET) and time integrated TTC (TIT), employing the threshold TTC* to differentiate between secure and hazardous conditions [50].

TET measures the total time vehicles are in hazardous traffic, marked by TTC below the set TTC*. Essentially, it sums up the time each vehicle spends potentially colliding with the one in front when TTC is under TTC*. $TET(t)$ can be calculated precisely using *Equation 15*;

$$TET(t) = \sum_{n=1}^{N} \delta_n^t, \qquad \delta_n^t = \begin{cases} 1, & (if\ 0 < TTC_n(t) \leq TTC^*) \\ 0, & (otherwise) \end{cases} \tag{15}$$

where δ_n^t is a 0-1 variable, N is the total number of vehicles.

TIT is calculated as the accumulation of TTC values. It reflects the variation in safety levels across different TTC instances that fall beneath the specified threshold TTC^*. Consistent with TET, the larger TIT represents a higher collision risk. The value of $TIT(t)$ is determined using *Equation 16*.

$$TIT(t) = \sum_{n=1}^{N} (TTC^* - TTC_n(t)), \qquad TTC^* > TTC_n(t) \tag{16}$$

Simulation experiments were carried out to analyse the safety indicators of the three models respectively. Referring to existing research, the value of TTC^* ranges from 1 to 3 seconds [44, 45]. Then TTC^* was set to 1 s, 2 s and 3 s, respectively, in the experiment. The results obtained are shown in *Figure 7*.

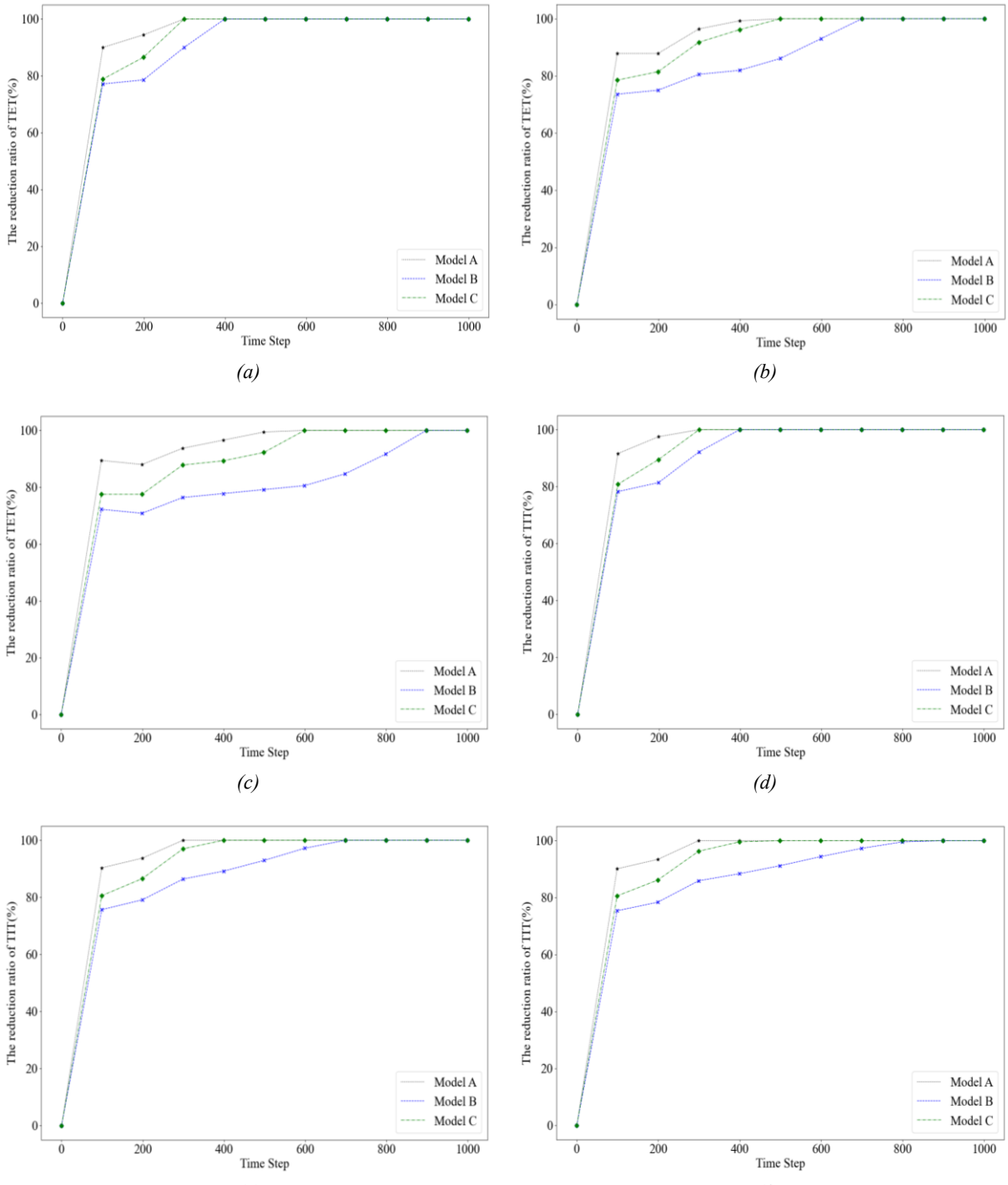

Figure 7 – TET and TIT indicators with different TTC thresholds: a) TET with $TTC^* = 1\ s$; b) TET with $TTC^* = 2\ s$; c) TET with $TTC^* = 3s$;d) TIT with $TTC^* = 1\ s$; e) TIT with $TTC^* = 2s$; f) TIT with $TTC^* = 3\ s$

As shown in *Figure 7*, *Figures 7a-7c* display the reduction ratio of TET values of the three different models when different TTC* values were taken within 1,000 simulation seconds. *Figures 7d-7f* show the reduction ratio of TIT values of the three different models with different TTC* values. The curves of different colours in the figure represent different models. It can be seen from *Figures 7a-7c* that the TET reduction ratio of Model A reaches first. Moreover, the values of the TET reduction ratio of Model A are larger than those of the other two models before reaching 100%. It can be seen from *Figures 7d-7f* that TIT and TET have the same variation patterns, indicating that Model A exhibits better safety performance compared with the other two models. The threshold TTC* exerts minimal influence on the reduction ratio of both TET and TIT, and the variation trends of TET and TIT remain consistent across the same models. Because better traffic safety performance makes the missing information less significant, the conclusion from the traffic safety perspective aligns with the findings of the previous two sections.

7. CONCLUSION

The V2X technology provides great convenience for obtaining various information that influences car-following behaviours. Then, multi-source information fusion models are required for description. Furthermore, too much information may increase the processing time and processing complexity. Then the impact of each information item needs to be investigated. Based on these, the objective of this research is to develop an integrated model framework designed to understand vehicle following behaviours within a vehicle-to-everything (V2X) setting, and to evaluate the impact of diverse information types on the model's performance. This initiative is expected to offer valuable perspectives and guidance for the advancement of future intelligent transportation systems.

Firstly, a comprehensive review of the literature is conducted to establish an integrated car-following model framework. Subsequently, referring to existing studies, based on the BLVD model, an integrated model in the V2X environment is established by integrating the information identified, which is named the BL-MSIF model.

Then, the performance of the BL-MSIF model is assessed by utilising numerical simulation. The simulation experiments demonstrate that the BL-MSIF model improves traffic stability in both circular road and straight road scenarios. The result lays a certain foundation for the construction of car-following models in the era of connected vehicles.

Finally, based on the integrated model framework, the contributions of various information items to the model are examined through comparative analysis from three perspectives: traffic flow stability, additional energy consumption and traffic safety. The results indicate that the acceleration information of preceding vehicles holds the highest importance, while the contribution of driver memory effect information to the model is relatively low, which offers insights for information transmission in connected vehicles.

However, there are certain limitations. Firstly, due to the influence of real vehicle testing conditions, the improved following model was not tested with real vehicles. Secondly, there has been a lack of investigation into how the model performs under mixed traffic conditions, specifically when both connected vehicles and those operated by humans are present. The next step is to conduct real vehicle testing to further optimise the model and investigate its characteristics in heterogeneous traffic flow. At present, only limited information is available, but as more data become accessible, increasingly advanced and comprehensive models will be developed in the future.

ACKNOWLEDGEMENTS

The authors would like to acknowledge the financial support for this study provided by the National Natural Science Foundation of China (No. 72161032), the Inner Mongolia Natural Science Foundation (No. 2025MS05010) and the Program for Young Talents of Science and Technology, China (No. NJYT22099).

REFERENCES

[1] Jiang LJ, Molnár TG, Orosz G. On the deployment of V2X roadside units for traffic prediction. *Transport. Res. Part C: Emerg. Technol*. 2021;129:103238. DOI: 10.1016/j.trc.2021.103238.

[2] Ma FW, et al. Eco-driving-based cooperative adaptive cruise control of connected vehicles platoon at signalized intersections. *Transport. Res. Part D: Transport and Environment*. 2021;92:102746. DOI: 10.1016/j.trd.2021.102746.

[3] Li M, et al. An eco-driving system for electric vehicles with signal control under a V2X environment. Transport. *Res. Part C: Emerg. Technol*. 2018;93:335-350. DOI: 10.1016/j.trc.2018.06.002.

[4] Li GF, et al. Decision making of autonomous vehicles in lane change scenarios: Deep reinforcement learning approaches with risk awareness. *Transport. Res. Part C: Emerg. Technol*. 2022;134:103452. DOI: 10.1016/j.trc.2021.103452.

[5] Du YC, et al. Decision making of autonomous vehicles in lane change scenarios: Deep reinforcement learning approaches. Comfortable and energy-efficient speed control of autonomous vehicles on rough pavements using deep reinforcement learning. *Transport. Res. Part C: Emerg. Technol*. 2022;134:103489. DOI: 10.1016/j.trc.2021.103489.

[6] He YM, et al. Modeling and simulation of lane-changing and collision avoiding autonomous vehicles on superhighways. *Physica A: Statistical Mechanics and its Applications*. 2023;609:128328. DOI: 10.1016/j.physa.2022.128328.

[7] Jing P, et al. Listen to social media users: Mining Chinese public perception of automated vehicles after crashes. *Transport. Res. Part F: Traffic Psychology and Behaviour*. 2023;93:248-265. DOI: 10.1016/j.trf.2023.01.018.

[8] Han JY, et al. The Car-following model and its applications in the V2X environment: A historical review. *Future Internet*. 2022;14(1),14. DOI: 10.3390/fi14010014.

[9] Sun YQ, Ge HX, Cheng RJ. An extended car-following model under V2V communication environment and its delayed-feedback control. *Physica A: Statistical Mechanics and its Applications*. 2018;508:349-358. DOI: 10.1016/j.physa.2018.05.102.

[10] Peng Y, Liu SJ, Yu DZ. An improved car-following model with consideration of multiple preceding and following vehicles in a driver's view. *Physica A: Statistical Mechanics and its Applications*. 2020;538:122967. DOI: 10.1016/j.physa.2019.122967.

[11] Peng GH, et al. Integrating the historical evolution information integral effect in car-following model under the V2X environment. *Physica A: Statistical Mechanics and its Applications*. 2023;627:129125. DOI: 10.1016/j.physa.2023.129125.

[12] Dangi R, Redhu P. Analyzing the impact of nearby information of vehicles on a car-following model in a V2X communication with passing. *International Journal of Non-Linear Mechanics.* 2025;175:105113. DOI: 10.1016/j.ijnonlinmec.2025.105113.

[13] Yadav D, Siwach V, Redhu P. The interplay of passing, driver attention, and cyber attack-induced information delays on traffic stability. *Chaos Solitons & Fractals.* 2025;196:116366. DOI: 10.1016/j.chaos.2025.116366.

[14] Yadav S, Redhu P. Self-stabilization control on traffic flow of connected and automated vehicles under cyberattacks. *European Physical Journal Plus.* 2023;138(12):1160. DOI: 10.1140/epjp/s13360-023-04791-8.

[15] Yadav S, Redhu P. Bifurcation analysis of driver's characteristics in car-following model. *Journal of Computational and Nonlinear Dynamics.* 2023;18(11):114501. DOI: 10.1115/1.4063338.

[16] Siwach V, Yadav D, Redhu P. Enhancing driver's attention and overtaking efficiency in car-following model for Advanced Driver Assistance Systems (ADAS) vehicles. *Physica a-Statistical Mechanics and Its Applications.* 2025;657:130207. DOI: 10.1016/j.physa.2024.130207.

[17] Yadav D, et al. Analyzing the impact of visibility, driver attentiveness, and energy consumption in severe weather in the car-following scenario under V2X environment. *Indian Journal of Physics.* 2025. DOI: 10.1007/s12648-024-03535-3.

[18] Tang TQ, et al. An extended car-following model with consideration of the reliability of inter-vehicle communication. *Measurement*. 2014;58:286-293. DOI: 10.1016/j.measurement.2014.08.051.

[19] Lenz H, Wagner CK, Sollacher R. Multi-anticipative car-following model. *European Physical Journal B*. 1999;7(2):331-335. DOI: 10.1007/s100510050618.

[20] Wang T, Gao ZY, Zhao XM. Multiple velocity difference model and its stability analysis. *Acta Physica Sinica*. 2006;55(2):634-640. DOI: 10.7498/aps.55.634.

[21] Peng GH, Sun DH. A dynamical model of car-following with the consideration of the multiple information of preceding cars. *Physics Letters A*. 2010;374(15-16):1694-1698. DOI: 10.1016/j.physleta.2010.02.020.

[22] Sun DH, Li YF, Tian C. Car-following model based on the information of multiple ahead & velocity difference. *Systems Engineering-Theory and Practice*. 2010;30(7):1326- 1332.

[23] Sun DH, Liao XY, Peng GH. Effect of looking backward on traffic flow in an extended multiple car-following model. *Physica A: Statistical Mechanics and its Applications*. 2011;390(4):631-635. DOI: 10.1016/j.physa.2010.10.016.

[24] Ma DF, et al. Modeling and analysis of car-following behavior considering backward-looking effect. *Chinese Physics B*. 2021;30(3):034501. DOI: 10.1088/1674-1056/abc3b3.

[25] Ma DF, et al. Nonlinear analysis of the car-following model considering headway changes with memory and backward looking effect. *Physica A: Statistical Mechanics and its Applications*. 2021;562:125303. DOI: 10.1016/j.physa.2020.125303.

[26] Wang QY, Ge HX. An improved lattice hydrodynamic model accounting for the effect of "backward looking" and flow integral. *Physica A: Statistical Mechanics and its Applications*. 2019;513:438-446. DOI: 10.1016/j.physa.2018.09.025.

[27] Qi XY, Cheng RJ, Ge HX. Nonlinear analysis of a new two-lane lattice hydrodynamic model accounting for "backward looking" effect and relative flow information. *Modern Physics Letters B*. 2019;33(19):1950223. DOI: 10.1142/s0217984919502233.

[28] Peng GH, et al. Optimal velocity difference model for a car-following theory. *Physics Letters A*. 2011;375(45):3973-3977. DOI: 10.1016/j.physleta.2011.09.037.

[29] Cao JL, Shi ZK, Zhou J. An extended optimal velocity difference model in a cooperative driving system. *International Journal of Modern Physics C*. 2015;26(5):1550054. DOI: 10.1142/s0129183115500540.

[30] Li XY, Zhou T, Yang ZY. Car-following model based on the information of the nearest-neighbor leading car's acceleration. *Journal of Chongqing University*. 2015;38:153-158. DOI: 10.11835/j.issn.1000-582X.2015.06.021.

[31] Yu SW, Shi ZK. An extended car-following model at signalized intersections. *Physica A: Statistical Mechanics and its Applications*. 2014;407:152-159. DOI: 10.1016/j.physa.2014.03.081.

[32] Herman R, et al. Traffic dynamics: Analysis of stability in car following. *Operations Research*. 1959;7(1):86-106. DOI: 10.1287/opre.7.1.86.

[33] Yu SW, Shi ZK. The effects of vehicular gap changes with memory on traffic flow in cooperative adaptive cruise control strategy. *Physica A: Statistical Mechanics and its Applications*. 2015;428:206-223. DOI: 10.1016/j.physa.2015.01.064.

[34] Kuang H, et al. An extended car-following model incorporating the effects of driver's memory and mean expected velocity field in ITS environment. *International Journal of Modern Physics C*. 2021;32(07):2150095. DOI: 10.1142/s0129183121500959.

[35] Peng GH, et al. Nonlinear analysis of a new car-following model accounting for the optimal velocity changes with memory. *Communications in Nonlinear Science and Numerical Simulation*. 2016;40:197-205. DOI: 10.1016/j.cnsns.2016.04.024.

[36] Yu SW, Zhao XM, Xu ZG, Zhang LC. The effects of velocity difference changes with memory on the dynamics characteristics and fuel economy of traffic flow. *Physica A: Statistical Mechanics and its Applications*. 2016;461:613-628. DOI: 10.1016/j.physa.2016.06.060.

[37] Shah D, Lee C, Kim YH. Modified Gipps model: A collision-free car following model. *Journal of Intelligent Transportation Systems*, 2023. DOI: 10.1080/15472450.2023.2289149.

[38] Colombaroni C, Fusco G. Artificial neural network models for car following: Experimental analysis and calibration issues. *Journal of Intelligent Transportation Systems*. 2014;18(1):5-16. DOI: 10.1080/15472450.2013.801717.

[39] Jiang R, Wu QS, Zhu ZJ. Full velocity difference model for a car-following theory. *Physical Review E*. 2001;64(1):017101. DOI: HTTPS://DOI.ORG/10.1103/PhysRevE.64.017101.

[40] Sun DH, et al. Effect of backward looking and velocity difference in an extended car following model. *Journal of Sichuan University*. 2012;49:115-120. DOI: 10.3969/j.issn.0490-6756.2012.01.019.

[41] Li X, et al. Numerical simulation of car-following model considering multiple-velocity difference and changes with memory. International Conference on Electronics, *Communications and Information Technology (CECIT)*. 2021;777-782.

[42] Qin YY, Wang H. Stabilizing mixed cooperative adaptive cruise control traffic flow to balance capacity using car-following model. *Journal of Intelligent Transportation Systems*. 2023;17(1):57-79. DOI: 10.1080/15472450.2021.1985490.

[43] Khound P, et al. Extending the adaptive time gap car-following model to enhance local and string stability for adaptive cruise control systems. *Journal of Intelligent Transportation Systems*. 2023;27(1/6):36-56. DOI: 10.1080/15472450.2021.1983810.

[44] Li ZB, et al. Development of a variable speed limit strategy to reduce secondary collision risks during inclement weathers. *Accident Analysis & Prevention*. 2014;72:134-145. DOI: 10.1016/j.aap.2014.06.018.

[45] Li Y, et al. Reducing the risk of rear-end collisions with infrastructure-to-vehicle (I2V) integration of variable speed limit control and adaptive cruise control system. *Traffic Injury Prevention.* 2016;17(6):597-603. DOI: 10.1080/15389588.2015.1121384.

[46] Tang TQ, Yu Q. Influences of vehicles' fuel consumption and exhaust emissions on the trip cost without late arrival under car-following model. *International Journal of Modern Physics C*. 2016;27(1):1650011. DOI: 10.1142/s012918311650011x.

[47] Peng GH, et al. CO2 emission control in new CM car-following model with feedback control of the optimal estimation of velocity difference under V2X environment. *Chinese Physics B.* 2021;30(10):108901. DOI: 10.1088/1674-1056/ac1417.

[48] Peng GH, et al. A novel car-following model by sharing cooperative information transmission delayed effect under V2X environment and its additional energy consumption. *Chinese Physics B*. 2022;31(5):058901. DOI: 10.1088/1674-1056/ac422a.

[49] Oguchi T, Katakura M, Taniguchi M. Carbondioxide emission model in actual urban road vehicular traffic conditions. *Proceedings of JSCE.* 2002;(695):125-136. DOI: 10.2208/jscej.2002.125.

[50] Minderhoud MM, Bovy PH. Extended time-to-collision measures for road traffic safety assessment. *Accident Analysis & Prevention*. 2001;33(1):89-97. DOI: 10.1016/S0001-4575(00)00019-1.